Heat Conductor Model for the Component Thermal-Hydraulic Analysis Module, CUPID

H. K. Cho* , I. K. Park, H. Y. Yoon, J. Kim, J. J. Jeong
Korea Atomic Energy Research Institute,1045 Daedeok-daero, Yuseong-gu, Daejon, 305-353,Korea
**Corresponding author*: hkcho@kaeri.re.kr

1. Introduction

A thermal-hydraulic analysis module, CUPID has been developed for a design and safety analysis of a nuclear reactor component [1]. In the CUPID code, a two-fluid three-field model is adopted and the governing equations are solved on an unstructured grid to make CUPID advantageous for a flow analysis in complicated geometries. As for the numerical solution scheme, the semi-implicit method was adopted, which has proved to be stable and accurate for most applications of a nuclear reactor transient.

A thermal analysis of a heat structure in a nuclear reactor component is very important for the safety analysis of a nuclear reactor as well as that of a fluid. Moreover, a conjugate heat transfer analysis between a fluid and a heat structure is indispensible in many transient situations of a nuclear reactor. For this reason, a heat conductor model was implemented into the CUPID module in this study. This paper presents the governing equation, numerical method and verification results of the heat conductor model.

2. Heat Conductor Model

2.1 Governing Equation and Numerical Method

The integral form of the heat conduction equation is

$$\int \rho_s C_{P,s} \frac{\partial T_s}{\partial t} dV = \int \nabla \cdot k_s \nabla T_s dV + \int q_s''' dV + \int q_{f-s}'' dA \qquad (1)$$

where, s :solid and f : fluid.

Each term of the heat conduction equation can be discretized with the finite volume method. The conduction of heat is discretized implicitly and the heat transfer on a solid-fluid interfaces explicitly.

$$\int \rho_s C_{P,s} \frac{\partial T_s}{\partial t} dV = \rho_s C_{P,s} \frac{T_s^{n+1} - T_s}{\Delta t} V_{cell} \qquad (2)$$

$$\int \nabla \cdot k_s \nabla T_s dV = \sum_f \left\{ (k_s)_f \left[\frac{\left(T_{s,j}^{n+1} - T_{s,i}^{n+1}\right) S_f}{\left(\vec{D}_{ji} \cdot \vec{n}\right)_f} + \left(\overline{\nabla T_s} \cdot \vec{n}\right)_f S_f - \frac{\left(\overline{\nabla T_s} \cdot \vec{D}_{ji}\right)_f S_f}{\left(\vec{D}_{ji} \cdot \vec{n}\right)_f} \right] \right\} \qquad (3)$$

$$\int q_s''' dV = q_s''' V_{cell} \qquad (4)$$

$$\int q_{f-s}'' dA = \sum_f \left(q_{f-s}''\right)_f S_f \qquad (5)$$

The subraction of second and third terms in the right hand side of Eq. (3) is a cross diffusion of the conductive heat, which is induced by a non-orthogonality of a mesh.

Substituting Eqs. (2)~(5) into Eq. (1) and rearranging the equation, we obtain

$$T_s^{n+1} - \sum_f \left\{ \frac{(k_s)_f \cdot \Delta t \cdot S_f}{\left(\rho_s C_{P,s} V_{cell}\right)_i \cdot \left(\vec{D}_{ji} \cdot \vec{n}\right)_f} \left(T_{s,j}^{n+1} - T_{ss,i}^{n+1}\right) \right\} = \sum_f \left\{ \frac{(k_s)_f \cdot \Delta t \cdot S_f}{\left(\rho_s C_{P,s} V_{cell}\right)_i} \cdot \overline{\nabla T_s} \cdot \left(\vec{n} - \vec{D}_{ji} / \left(\vec{D}_{ji} \cdot \vec{n}\right)_f\right)_f \right\} + \frac{q_s''' \Delta t}{\rho_s C_{P,s}} + \frac{\sum_f \left(q_{f-s}''\right)_f S_f}{\left(\rho_s C_{P,s} V_{cell}\right)} + T_s \cdot \qquad (6)$$

A N×N system of linear algebraic equations are established by considering N conductor cells as follows,

$$\begin{pmatrix} \left[1 + \sum_f (AA)_f\right]_1 & \cdots & -(AA)_{1,m} & \cdots & -(AA)_{1,N} \\ \vdots & \ddots & \vdots & & \vdots \\ -(AA)_{i,1} & \cdots & \left[1 + \sum_f (AA)_f\right]_i & \cdots & -(AA)_{i,N} \\ \vdots & & \vdots & \ddots & \vdots \\ -(AA)_{N,1} & \cdots & -(AA)_{N,m} & \cdots & \left[1 + \sum_f (AA)_f\right]_N \end{pmatrix} \begin{pmatrix} T_{s,1}^{n+1} \\ \vdots \\ T_{s,i}^{n+1} \\ \vdots \\ T_{s,N}^{n+1} \end{pmatrix} = \begin{pmatrix} BB_1 \\ \vdots \\ BB_i \\ \vdots \\ BB_N \end{pmatrix}. \qquad (7)$$

The coefficient matrix of Eq. (7) is sparse because an unstructured grid is used for the present solver. However, it is a symmetric matrix so that the ICCG (Incomplete Cholesky Conjugate Gradient) can be applied to perform the matrix inversion, which is beneficial in terms of fast convergence for symmetric matrices [2].

2.2 Fluid-solid Interface

For the conjugate heat transfer analysis between fluids and solids, the following energy conservation relation was used to determine the interface temperature (Fig. 1).

$$q_1'' = -q_2'' = k_1 \frac{\left(T_{f-s}\right)_f - T_1}{\Delta x_1} = -k_2 \frac{\left(T_{f-s}\right)_f - T_2}{\Delta x_2} \qquad (8)$$

Rearranging Eq. (8), the fluid-solid interface temperature can be obtained

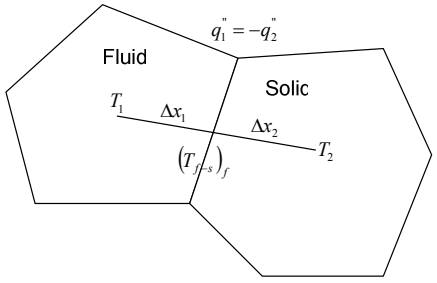

Fig. 1 Control Volume of Fluid-Solid Interface

$$\left(T_{f-s}\right)_f = \frac{k_1\Delta x_2 T_1 + k_2\Delta x_1 T_2}{\left(k_1\Delta x_2 + k_2\Delta x_1\right)} = \frac{k_1 \cdot fac1 \cdot T_1 + k_2 \cdot fac \cdot T_2}{\left(k_1 \cdot fac1 + k_2 \cdot fac\right)} \quad (9)$$

where $fac1 = \Delta x_2 /(\Delta x_1 + \Delta x_2)$ and $fac = \Delta x_1 /(\Delta x_1 + \Delta x_2)$.

In the case of a two-phase flow, a heat partitioning factor is necessary to distribute the energy transferred from solids to each phase properly. For this, the following simple heat partitioning factor was implemented in the present solver.

$$Part_l = \begin{cases} 1 & if\ \ \alpha_g < 0.9 \\ 1 - 10 \cdot (\alpha_g - 0.9) & if\ \ 0.9 \le \alpha_g \le 1 \end{cases} \quad (10)$$

This will be revised in the future with physically reasonable models.

Finally, considering the heat partitioning factor, Eq. (9) becomes

$$\left(T_{f-s}\right)_f = \frac{fac1 \cdot \left[Part_l \cdot k_l T_l + \left(1 - Part_l\right) \cdot k_g T_g\right] + fac \cdot k_s T_{s,i}}{fac1\left[Part_l \cdot k_l + \left(1 - Part_l\right) \cdot k_g\right] + fac \cdot k_s}. \quad (11)$$

3. Calculation Results for a Verification

For the verification of the conductor model of the CUPID module, two preliminary calculations were performed. One is for the heat conduction in a solid and the other for the fluid-solid conjugate heat transfer.

Fig. 2 shows the meshes used for the conduction equation solver verification (Problem-1). Both structured mesh and unstructured mesh were used for the calculations. For the boundary conditions, a constant temperature wall ($T_1 = 400K$) condition was imposed on Boundary 1 and adiabatic walls on Boundaries 2, 3 and 4. A volumetric heat source ($q''' = 10kW/m^3$) was applied to the problem. In Fig. 3, the CUPID calculation results were compared with the analytical solution. As shown in the figure, the calculation results of CUPID are well correspondent with the analytical solution on both structured and unstructured meshes.

The other verification problem (Problem-2) was the 2D-laminar flow heat transfer with two solid walls. Fig. 4 shows the mesh of the calculation, the imposed boundary conditions and the properties of the fluid and solid. In Fig. 5, the temperature distributions in the calculation were compared with the analytical solutions. The comparison of the results showed a good agreement between the calculation and the analytical solution.

From these verification results, it was concluded that the conductor model of the CUPID module was well established and implemented.

4. Conclusion

The governing equation, numerical method and the preliminary calculation results for the verification of the CUPID conductor model are introduced in this paper. The heat partitioning factor will be implemented based on physical models instead of the simple model and various calculations for its validation will be performed.

[1] J.J. Jeong et al., A Semi-implicit Numerical for a Transient Two-fluid Three-field Model on an unstructured grid, Int. Comm. Heat and Mass Tran., 35, pp. 597-605, 2008.
[2] D. S. Kershaw, The Incomplete Cholesky-Conjugate Gradient Method for the Iterative Solution of Systems of Linear Equations, Journal of Computational Physics, 26, pp. 43–65, 1978.

Acknowledgements

This study has been carried out under the nuclear R&D program by the Korean Ministry of Education, Science and Technology.

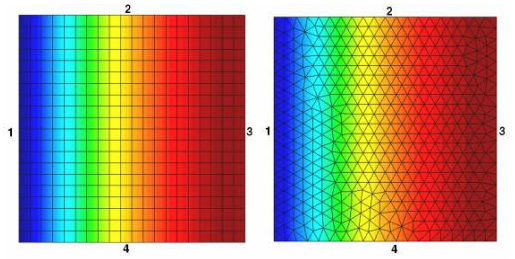

Fig. 2 Meshes and Calculation Results for Problem-1

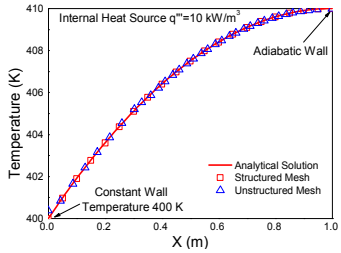

Fig. 3 Calculation Results for Problem-1

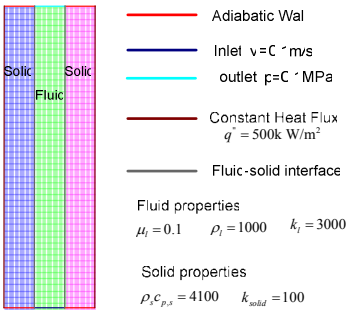

Fig. 4 Mesh and Boundary Conditions for Problem-2

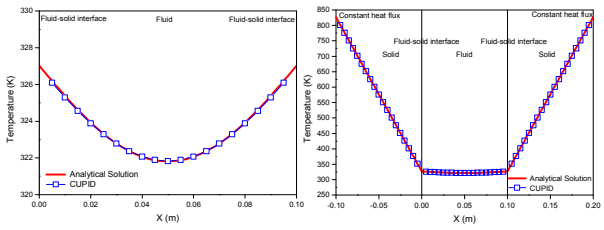

(a) Fluid Temperature (b) Solid and Fluid Temperature

Fig. 5 Calculation Results for Problem-2